Theory of the photon-drag effect in simple metals

John Eric Goff and W. L. Schaich
Department of Physics, Indiana University, Bloomington, Indiana 47405
(Received 2 July 1999)

We derive and evaluate a quantum mechanical, self-consistent field theory of the photon-drag effect in simple metals. The calculation of the induced voltage across a flat surface illuminated with light is based on a scheme that allows the separate treatment of contributions that depend on bulk or surface response properties. The microscopic theory uses the time-dependent local density-functional approach in a numerical formulation similar to that for second harmonic generation, but incorporates finite damping. The results show a considerable sensitivity to the surface behavior of the responding electrons, with the strength of the surface contribution increased by two orders of magnitude compared to an earlier hydrodynamic estimate.

I. INTRODUCTION

In this paper we complete the development of a theory of photon-drag effects in simple metals. Our goal has been to derive results at the same level of sophistication and accuracy as has been worked out for second harmonic generation (SHG).[1,2] Many of the details are quite different because the experimental phenomena are so distinct. For SHG one seeks to describe radiation patterns, while photon drag involves dc effects: induced currents and voltages. Still there are fundamental similarities in their analysis because both sets of phenomena arise from the second-order response of electrons near an interface to an applied field.

In an earlier paper[3] we examined photon-drag effects within a hydrodynamic model of the electrons' dynamics. Such a model is crude but tractable and allowed us to approach the problem at different levels of approximation. From this analysis we established the reasonable accuracy of the following parametrization scheme. Consider a wide beam of monochromatic light incident at angle θ on a flat surface of jellium metal. A steady current flowing parallel to the surface is induced, along with a dc voltage difference along the surface normal. If the resistive scattering rate for the electrons does not vary with position near the surface, the time-averaged current per unit width (of the incident light beam) may be found from[3,4]

$$\int dx\langle J_{\parallel}\rangle = \sigma_0\left(\frac{\langle S\rangle}{n_b e c}\right)\sin\theta\cos\theta(1-R), \tag{1}$$

where $\langle S\rangle$ is the time-averaged incident Poynting flux, R the light's reflection coefficient, and σ_0 the metal's dc conductivity, $\sigma_0 = n_b e^2 \tau_b / m$ with n_b and $1/\tau_b$ the bulk electron density and scattering rate, respectively. The other variables in Eq. (1) are fundamental constants for an electron, $e<0$ and m, and the speed of light c. The variable of integration, x, represents the normal coordinate. The reflection coefficient depends on the polarization of the light and may be calculated from classical (local) optics. The contributions to $\int dx\langle J_{\parallel}\rangle$ from s- and p-polarized light add without interference. Equation (1) is straightforward to evaluate and, as long as $1/\tau$ is spatially constant, should be accurate to within a few percent. Specifically, corrections due to nonlocal optics should not be significant.[3]

Matters are different for the induced voltage across the surface. This is defined by $\langle \Delta\mathcal{E}\rangle = -\int dx\langle E_{\rm ind}\rangle$, where $\langle E_{\rm ind}\rangle$ is the time-averaged field normal to the surface produced at second order by the charge redistribution. Under the same assumptions that lead to Eq. (1) we showed that[3]

$$\langle \Delta\mathcal{E}\rangle = \frac{\langle S\rangle}{n_b e c}\Gamma_x, \tag{2}$$

with $\Gamma_x^{(s)} = (1+R_s)\cos^2\theta$ for s waves while for p polarization

$$\Gamma_x^{(p)} = (1+R_p)\cos^2\theta + (\tfrac{1}{2}+2h)\left|t_p \sin\theta(\epsilon_b - 1)\right|^2. \tag{3}$$

Here ϵ_b is the bulk dielectric function, t_p the Fresnel transmission amplitude for a p wave, and h a real-valued dimensionless parameter that requires microscopic evaluation. Except for h, the ingredients of Eq. (2) are just as easy to calculate as those in Eq. (1) and the accuracy should also be at the few percent level. The parameter h, however, requires a nonlocal response calculation and its magnitude is quite sensitive to the microscopic description of the surface.

It was further demonstrated in Ref. 3 that h may be found from a one-dimensional, electrostatic calculation. Consider the application of an electric field along the surface normal, with a spatially uniform amplitude E_A and frequency ω. The electrons' response to this field will produce at first order an induced surface charge density $\mathrm{Re}[\sigma_1 e^{-i\omega t}]$ and at second order an induced density profile from which one extracts the time-averaged, but spatially varying part $\langle \rho_2(x)\rangle$. Then h is given by

$$h = e n_b \int dx x\langle \rho_2(x)\rangle / |\sigma_1|^2. \tag{4}$$

Throughout this recipe for h, one may set $c\to\infty$ and ignore magnetic fields. Thus a nonretarded, density response calculation suffices to determine h and the result depends only on ω, and not on θ. Within the hydrodynamic model we checked that this relatively simple prescription can reasonably reproduce a full evaluation of $\Gamma_x^{(p)}$.[3] Since the importance of retardation (finite c) should not depend on whether

 ©2000 The American Physical Society

one is using hydrodynamics or quantum mechanics to describe the near-surface response, we shall use here the prescription (4) in a quantum mechanical calculation.

The spirit of our approach is very similar to that used in second harmonic generation, where in the simplest jellium model the full result is determined by several macroscopic parameters (θ, ϵ_b, polarization) and one complex-valued, dimensionless parameter which is sensitive to the microscopic surface physics. This parameter is called a and in our notation it is determined by

$$a = 8en_b \int dx x \rho_2(x,2\omega)/\sigma_1^2, \tag{5}$$

where $\rho_2(x,2\omega)$ is the complex amplitude of the nonretarded induced charge density at second order with frequency 2ω. The justification for this recipe also comes from hydrodynamic model calculations.[5] The equation where a appears in SHG (Refs. 1, 2, 5) is quite different in form from Eqs. (2),(3) where h appears, but the similarity of Eqs. (4),(5) is obvious and shows why the surface sensitivity of photon drag and SHG should be essentially the same.

So to complete our theory we need a microscopic, quantum-mechanical calculation of h. This will be done here within a time-dependent local density-functional approximation (TDLDA). In Sec. II we describe the formal response theory and how we set up its numerical evaluation. Detailed results are shown in Sec. III and we end in Sec. IV with a comparison of different microscopic estimates of h. This paper is focused on a particular calculational scheme. For a broader perspective on the photon-drag problem, the reader can consult Ref. 3 for citations that survey earlier work. Papers published since then include Refs. 6–8 but these mainly address photon-drag currents in quantum wells.

II. THEORY

A. Density-functional response

By using density-functional theory we are led to calculations of how a single electron moves in an effective potential energy V (Ref. 9)

$$V(x,t) = e\varphi(x,t) + \mu_{xc}[n(x,t)]. \tag{6}$$

For a jellium model and with the applied field normal to the surface, V depends only on the normal coordinate x and the time t. It has two distinct contributions. The first is from the Hartree potential, which obeys

$$\frac{d^2}{dx^2}\varphi(x,t) = -4\pi\rho(x,t), \tag{7}$$

and is a linear but nonlocal function of the charge density. The second is due to exchange and correlation effects and is to be calculated from

$$\mu_{xc}[n] = \frac{\partial}{\partial n}(n\epsilon_{xc}), \tag{8}$$

where ϵ_{xc} is the average exchange and correlation in a uniform electron gas of density n. We use the standard Hartree-Fock result for the exchange part[10] and Wigner's interpolation formula for the correlation part.[9] Note that μ_{xc} in Eq. (6) is a local but nonlinear function of the electron density.

Our aim is to use perturbation theory to calculate induced densities and for that we need to separate V into pieces of different order in the applied field, whose strength is $E_A(t)$. We write

$$V(x,t) = \sum_i V_i(x,t) = \sum_i e\varphi_i(x,t) + \sum_i \mu_{xc}^{(i)}(x,t), \tag{9}$$

with $i = 0,1,2,\ldots$. At zeroth order the potential energy is time independent with φ_0 determined by the total charge density

$$\rho_{\rm tot}^{(0)}(x) = \rho_0(x) - en_b\theta(x), \tag{10}$$

where $e<0$ and the (positive) jellium background sits in $x>0$. The other contribution to $V_0(x)$ is

$$\mu_{xc}^{(0)}(x) = \mu_{xc}[n_0(x)], \tag{11}$$

where $n_0(x) = \rho_0(x)/e$ is the ground state density of the electrons. One solves for n_0 by an iterative loop until self-consistency is obtained.[2,9,11]

At first order one has

$$\mu_{xc}^{(1)}(x,t) = \mu_{xc}'(x)\rho_1(x,t)/e, \tag{12}$$

where $\mu_{xc}'(x) = (\partial^2/\partial n^2)(n\epsilon_{xc})$, evaluated at $n = n_0(x)$. The Hartree potential has contributions from both the applied field $E_A(t)$ and the field produced by the first-order charge density, $\rho_1(x,t)$:

$$\varphi_1(x,t) = -xE_A(t) - 2\pi\int dx'|x-x'|\rho_1(x',t)$$

$$\sim -xE_{\rm in}(t) + 4\pi\int_x^{x_c} dx'(x-x')\rho_1(x',t). \tag{13}$$

The $\sim$ in the second line means that we have dropped a constant contribution, which cannot change the response. The $E_{\rm in}$ that appears here is the electric field deep inside the metal. We imagine that the metal is a thick slab that has been inserted between the (parallel) plates of a capacitor. The charge on the capacitor plates produces E_A, whose value does not depend on the metal slab. The field near the center of the slab (at x_c in our coordinates) is

$$E_{\rm in}(t) = E_A(t) + 4\pi\int_{x_v}^{x_c} dx'\rho_1(x',t) = E_A(t) + 4\pi\sigma_1(t). \tag{14}$$

We assume the slab is thick enough that ρ_1 is negligible near x_c. It also vanishes near x_v, which is in the vacuum outside the metal but still between the capacitor plates. Although our interest is in the induced charge density on the left side of the slab (near $x=0$), to derive Eq. (14) one must acknowledge that a charge density of opposite sign is induced simultaneously ($c\to\infty$) on the right side of the slab.

At second order one has

$$\mu_{xc}^{(2)}(x,t) = \mu_{xc}'(x)\rho_2(x,t)/e + \tfrac{1}{2}\mu_{xc}''(x)[\rho_1(x,t)/e]^2, \tag{15}$$

where $\mu''_{xc}(x)=(\partial^3/\partial n^3)(n\epsilon_{xc})$ evaluated at $n=n_0(x)$. The Hartree potential is determined solely by the electron charge density $\rho_2(x,t)$:

$$\varphi_2(x,t)=4\pi\int_x^{x_c}dx'(x-x')\rho_2(x',t). \tag{16}$$

To derive this result we have used the assumption that no net charge is induced in second order near either surface; i.e.,

$$\int_{x_v}^{x_c}dx'\rho_2(x',t)=0. \tag{17}$$

This assumption fails above the threshold for photoemission due to the outgoing stream of electrons that extends indefinitely far into vacuum. We consequently shall not evaluate ρ_2 and h above the vacuum threshold. There is no such constraint on a and SHG because at 2ω, ρ_2 always vanishes in vacuum.

So far we have allowed for a general time dependence. Now we specialize to the monochromatic case $E_A(t)\rightarrow E_A e^{\gamma t}\cos\omega t$ with E_A real and γ positive. The factor $e^{\gamma t}$ slowly turns on the perturbation, whose effect we examine near $t=0$. We find at first order with $\rho_1(x,t)\rightarrow\frac{1}{2}[\rho_1(x,\omega)e^{-i\omega t}+\rho_1(x,-\omega)e^{i\omega t}]e^{\gamma t}$ and a similar form for V_1 that

$$\rho_1(x,\omega)=e\int dx'X_1(x,x';\omega)V_1(x',\omega). \tag{18}$$

The linear response matrix at zero temperature is determined by

$$X_1(x,x';\omega)=\frac{1}{\pi^2}\int_0^{k_F}dk(k_F^2-k^2)\psi_k(x)\psi_k(x')[G(x,x';\epsilon_k+\hbar(\omega+i\gamma))+G^*(x,x';\epsilon_k+\hbar(-\omega+i\gamma))], \tag{19}$$

where k_F is the Fermi wave vector, $\psi_k(x)$ a (real-valued) occupied wave function for motion along x and energy $\epsilon_k<\epsilon_F$, the Fermi energy, and G a one-body Green's function (see below). For second order matters are more complicated since the response is at both $\Omega=2\omega$ and $\Omega=0$. We write $\rho_2(x,t)\rightarrow\rho_2(x,0)e^{2\gamma t}+\frac{1}{2}[\rho_2(x,2\omega)e^{-2i\omega t}+\rho_2(x,-2\omega)e^{2i\omega t}]e^{2\gamma t}$ where $\rho_2(x,0)$ is real and the complex amplitudes obey $\rho_2(x,-2\omega)=\rho_2^*(x,2\omega)$.[12] Then response theory leads to[13,14]

$$\rho_2(x,\Omega=\omega_\alpha+\omega_\beta)=e\int dx'X_1(x,x';\Omega)V_2(x',\Omega)+\frac{e}{4}\sum_P\int dx_\alpha\int dx_\beta X_2(x,x_\alpha,x_\beta;\omega_\alpha,\omega_\beta)\times V_1(x_\alpha,\omega_\alpha)V_1(x_\beta,\omega_\beta). \tag{20}$$

The sum on P is over permutations of the variable pairs (x_α,ω_α) and (x_β,ω_β) and the new response matrix is

$$X_2(x,x_\alpha,x_\beta;\omega_\alpha,\omega_\beta)=\frac{1}{\pi^2}\int_0^{k_F}dk(k_F^2-k^2)(A_1+A_2+A_3), \tag{21}$$

with

$$A_1=G^*(x,x_\alpha;\epsilon_k+\hbar(-\omega_\alpha+i\gamma))\psi_k(x_\alpha)G(x,x_\beta;\epsilon_k+\hbar(\omega_\beta+i\gamma))\psi_k(x_\beta), \tag{22}$$

$$A_2=\psi_k(x)G(x,x_\alpha;\epsilon_k+\hbar(\Omega+2i\gamma))G(x_\alpha,x_\beta;\epsilon_k+\hbar(\omega_\beta+i\gamma))\psi_k(x_\beta), \tag{23}$$

$$A_3=\psi_k(x)G^*(x,x_\alpha;\epsilon_k+\hbar(-\Omega+2i\gamma))\times G^*(x_\alpha,x_\beta;\epsilon_k+\hbar(-\omega_\beta+i\gamma))\psi_k(x_\beta). \tag{24}$$

The Green's functions that appear here and in Eq. (19) are defined by

$$G(x,x';\epsilon+i\hbar\gamma)=\langle x|(\epsilon+i\hbar\gamma-h_0)^{-1}|x'\rangle, \tag{25}$$

with h_0 the (one-dimensional, one-body) ground state Hamiltonian. A more practical representation is as

$$G(x,x';\epsilon+i\hbar\gamma)=\frac{2m}{\hbar^2}\psi^>(x_>)\psi^<(x_<)/W, \tag{26}$$

where $x_{>_<}$ is the greater (lesser) of x,x' and W is the Wronskian of the two solutions at the complex energy $\epsilon+i\hbar\gamma$ which travel to the right ($\psi^>$) or to the left ($\psi^<$). As $x\rightarrow x_c$, $\psi^>(x)\rightarrow e^{iK_c x}$ while as $x\rightarrow x_v$, $\psi^<(x)\rightarrow e^{-iK_v x}$. Here $\hbar^2K_c^2/2m+V_0(x_c)=\epsilon+i\hbar\gamma$ while $\hbar^2K_v^2/2m+V_0(x_v)=\epsilon+i\hbar\gamma$, and both K_c and K_v have positive imaginary parts.

The numerical evaluation of Eqs. (18)–(26) is a long, detailed process and we checked at several stages that our results are consistent with the pioneering calculations of Feibelman[15] (at first order) and Liebsch[1,2] (at second order). Our approach differs from theirs in one important way. The damping parameter γ is not treated as infinitesimally small, but instead is set to a few percent of $\epsilon_F/\hbar$. This causes Friedel oscillations to damp more quickly as one moves into the bulk, which in turn stabilizes the numerics. The introduction of γ has the mathematical effect of making us calculate at complex-valued energies. The bulk dielectric function under this approximation appears as

$$\epsilon_b(\omega)=1-\omega_p^2/(\omega+i\gamma)^2, \tag{27}$$

where the square of the plasma frequency is $\omega_p^2=4\pi n_b e^2/m$. For $\gamma\ll\omega$ we can write

$$\epsilon_b(\omega\gg\gamma)\approx 1-\omega_p^2/[\omega(\omega+2i\gamma)], \tag{27'}$$

which is the Drude form with scattering rate $1/\tau=2\gamma$. So from this point of view, finite γ is allowing for incoherent scattering. However, the global replacement $\omega\rightarrow\omega+i\gamma$ is not a consistent treatment of such scattering.[16] For instance, as $\omega\rightarrow 0$, our $\epsilon_b\rightarrow+\omega_p^2/\gamma^2$, while the Drude $\epsilon_b\rightarrow+i\infty$. The numerical importance of such inconsistency is not clear. For the linear response d parameter we find for $\hbar\gamma/\epsilon_F\lesssim 0.02$ essentially the same results as those from codes where γ

$\rightarrow 0^+$.[2,15,17] As we will discuss in Sec. III there is a greater dependence on γ in second-order quantities.

B. Sum rules

Using the equations above we have numerically evaluated $\rho_2(x,\Omega)$ near the jellium surface. However, the calculation of h or a from Eqs. (4) or (5) is generally not reliable because of long-ranged Friedel oscillations. Fortunately it is possible to relate h and a to alternate integrals that are more tractable. We derive these here using the capacitor geometry.

The argument is based on calculating in different ways f_2, the (second-order) force per unit area on the left half of the jellium slab. We first write f_2 using the total electric field as

$$f_2 = \int_0^{x_c} dx E_2(x)(-e)n_b = e n_b \int_0^{x_c} dx \frac{\partial \varphi_2}{\partial x}(x), \quad (28)$$

where we have suppressed time arguments for the second-order amplitudes E_2 and φ_2. From Poisson's equation one can replace

$$\frac{\partial \varphi_2}{\partial x}(x) = -4\pi \int_{x_v}^{x} dx' \rho_2(x'), \quad (29)$$

where x_v is outside the metal. Because of Eq. (17), $\partial\varphi_2/\partial x$ vanishes near both x_v and x_c. Substituting Eq. (29) into Eq. (28) and reversing the integration order yields

$$f_2 = 4\pi e n_b \int_0^{x_c} dx' x' \rho_2(x') = m\omega_p^2 \int_0^{x_c} dx' x' n_2(x'). \quad (30)$$

The alternate route to f_2 writes it as the sum of the forces exerted by all the electrons in the slab on the nuclei (jellium) on the left side of the slab:

$$A f_2 = \sum F^{(2)}_{e \text{ on } n_l}, \quad (31)$$

where A is the slab's area. Using Newton's third law and Eq. (17), which implies that the second-order disturbance of electrons on the left (right) can produce no electric field nor feel a net force from charges on the right (left), we obtain

$$A f_2 = -\sum F^{(2)}_{n \text{ on } e_l}. \quad (32)$$

This expresses $-Af_2$ as the sum of forces exerted by all the nuclei (jellium) on the electrons on the left side of the slab.

We next want to reexpress Eq. (32) using Newton's second law, but must be careful with its form since the number of electrons on the left is changing in time. Begin with the sum of the (left-side) electrons' momenta: $(1/A)\Sigma p = \int_{x_v}^{x_c} dx n m v$. Since both n and v are space and time dependent,

$$\frac{d}{dt}\int_{x_v}^{x_c} dx n m v = \int_{x_v}^{x_c} dx n \frac{\partial (mv)}{\partial t} + \int_{x_v}^{x_c} dx m v \frac{\partial n}{\partial t} = \int_{x_v}^{x_c} dx n \frac{\partial (mv)}{\partial t} - \int_{x_v}^{x_c} dx m v \frac{\partial (nv)}{\partial x}, \quad (33)$$

where in the second line we have used the equation of continuity. Then integration by parts yields

$$\frac{d}{dt}\int_{x_v}^{x_c} dx n m v = -mnv^2\Big|_{x_v}^{x_c} + \int_{x_v}^{x_c} dx n \left(\frac{\partial}{\partial t} + v\frac{\partial}{\partial x}\right)(mv) = -m n_b v_c^2 + \int_{x_v}^{x_c} dx n F_{\text{tot}}. \quad (34)$$

Here we have replaced the total (convective) time derivative of mv by F_{tot}, the total force on an electron at x. The velocity of the electron fluid at x_c can be found from the rate of change of the number of electrons on the left,

$$\frac{d}{dt} N_1 = \frac{d}{dt}\int_{x_v}^{x_c} dx \rho_1 / e = -n_b v_c. \quad (35)$$

Now we use Eq. (34) at second order to reexpress Eq. (32) as

$$A f_2 = -\frac{d}{dt}\left(\sum p\right)^{(2)} - A m n_b v_c^2 + \sum F^{(2)}_{e \text{ on } e_l} + A\int_{x_v}^{x_c} dx \rho_1 E_A + A\int_{x_v}^{x_c} dx n_2 F_{\text{ext}}. \quad (36)$$

The last three terms here are additional forces that act on the electrons on the left side of the slab. For a complete TDLDA calculation F_{ext} vanishes, but if one omits exchange and correlation terms while calculating the first- and second-order responses, it is needed. We call such a calculation RPA for random phase approximation and one has $F^{(\text{RPA})}_{\text{ext}} = -\partial \mu^{(0)}_{xc}/\partial x$.[1,2] Since E_A is spatially constant, $\int_{x_v}^{x_c} dx \rho_1 E_A = \sigma_1 E_A$. The term with electron-electron forces nearly cancels out by action-reaction, except for the force on the first-order electron disturbance on the left due to the field $E_1^{r\to l}$ produced by the first-order electron disturbance on the right:

$$\sum F^{(2)}_{e \text{ on } e_l} = \sigma_1 E_1^{r\to l} = 2\pi\sigma_1^2. \quad (37)$$

Finally one may replace in second order $-(d/dt)(\Sigma p)^{(2)} = -(d^2/dt^2)(\Sigma m x)^{(2)}$.

To proceed further we need to be specific about the time dependencies. At first order we focus on quantities that vary at $\tilde{\omega} = \omega + i\gamma$. Then we can use Gauss's law to relate E_A to the complex amplitude σ_1,

$$4\pi\sigma_1 = E_{\text{in}} - E_A = E_A\left(\frac{1}{\epsilon_b} - 1\right) = \frac{-E_A}{(1 - \tilde{\omega}^2/\omega_p^2)}. \quad (38)$$

Moving to second order, we begin with SHG, where we seek the amplitude of $e^{-i\tilde{\Omega}t}$ with $\tilde{\Omega}=2\tilde{\omega}$. Combining Eq. (30) and (36),

$$(m\omega_p^2-m\tilde{\Omega}^2)\int_{x_v}^{x_c}dxxn_2(x)$$
$$=m\omega_p^2\int_{x_v}^{0}dxxn_2(x)+\frac{\sigma_1^2}{2}\left[\frac{4\pi}{\omega_p^2}\tilde{\omega}^2+2\pi-4\pi\times\left(1-\frac{\tilde{\omega}^2}{\omega_p^2}\right)\right]+\int_{x_v}^{x_c}dxn_2F_{\rm ext}. \quad (39)$$

The contributions in the square brackets simplify: $[]\rightarrow-2\pi(1-\tilde{\Omega}^2/\omega_p^2)$ so

$$\int_{x_v}^{x_c}dxxn_2(x)=-\frac{1}{4}\frac{\sigma_1^2}{n_be^2}+\left(1-\frac{\tilde{\Omega}^2}{\omega_p^2}\right)^{-1}\times\left(\int_{x_v}^{0}dxxn_2(x)+\int_{x_v}^{x_c}dxn_2F_{\rm ext}/m\omega_p^2\right). \quad (40)$$

Comparing with Eq. (5) we find the sum rule result

$$a=-2+8\left(1-\frac{\tilde{\Omega}^2}{\omega_p^2}\right)^{-1}\left(\int_{x_v}^{0}dxx\rho_2(x,\Omega)+\int_{x_v}^{x_c}dx\rho_2(x,\Omega)F_{\rm ext}(x)/m\omega_p^2\right)en_b/\sigma_1^2. \quad (41)$$

This is equivalent to the result in Ref. 2 and corrects the formula in Ref. 1.[18]

For photon drag the first order ingredients are the same, but at second order we need the amplitude of $e^{-i\tilde{\Omega}t}$ with $\tilde{\Omega}=2i\gamma$. The only formal change in Eq. (39) is with the square bracket terms which become real valued:

$$\frac{|\sigma_1|^2}{2}\left[-\frac{4\pi}{\omega_p^2}|\tilde{\omega}|^2+2\pi-4\pi\,{\rm Re}\left(1-\frac{\tilde{\omega}^2}{\omega_p^2}\right)\right]\rightarrow-\pi|\sigma_1|^2\left(1-\frac{\tilde{\Omega}^2}{\omega_p^2}\right). \quad (42)$$

Then a comparison with Eq. (4) yields the sum rule for h,

$$h=-\frac{1}{4}+\left(1+\frac{4\gamma^2}{\omega_p^2}\right)^{-1}\left(\int_{x_v}^{0}dxx\rho_2(x,0)+\int_{x_v}^{x_c}dx\rho_2(x,0)F_{ext}(x)/m\omega_p^2\right)en_b/|\sigma_1|^2. \quad (43)$$

As $\omega\rightarrow0$, $\rho_2(x,2\omega)\rightarrow\rho_2(x,0)$, and $h\rightarrow a/8$.[3] Furthermore, in a system that is strongly charged positive, ρ_2 becomes negligibly small before x has decreased to zero, so $h\rightarrow a/8\rightarrow-1/4$ for all frequencies (below the photoemission threshold).[3]

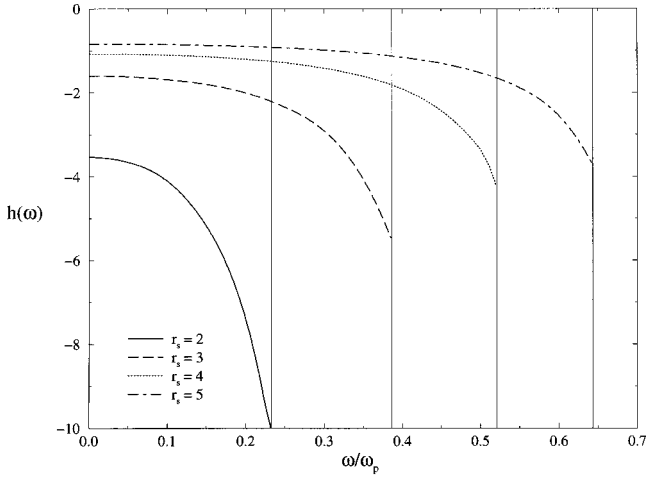

FIG. 1. Photon-drag h parameter versus frequency normalized to the bulk plasma frequency ω_p. The vertical lines locate the work function for the different values of r_s.

III. RESULTS

We begin with the overview of Fig. 1 which shows the photon drag h parameter evaluated from Eq. (44) as a function of the incident photon frequency for a sequence of metals. The (dimensionless) bulk density parameter[19] $r_s=2,3,4,5$ and in each case the damping is fixed at $\gamma=0.02\epsilon_{\rm F}/\hbar$. Results are shown only for frequencies up to the work function, which ranges from 3.9 eV for $r_s=2$ down to 2.7 eV for $r_s=5$. Over this range h shows remarkably little structure, simply decreasing monotonically from its zero frequency limit. We expect that h diverges at the photoemission threshold, but since the calculations are done with a fixed vacuum cutoff $k_{\rm F}x_v>-15$, we do not pick up the sudden onset of this divergence. Corresponding plots of the SHG a parameter show considerably more structure,[1,2] in part because the SHG response involves 2ω components while photon drag probes behavior only at ω and dc. Also, the a parameter spectrum extends beyond the photoemission threshold.

Moving back in the calculation, we show in Fig. 2 profiles

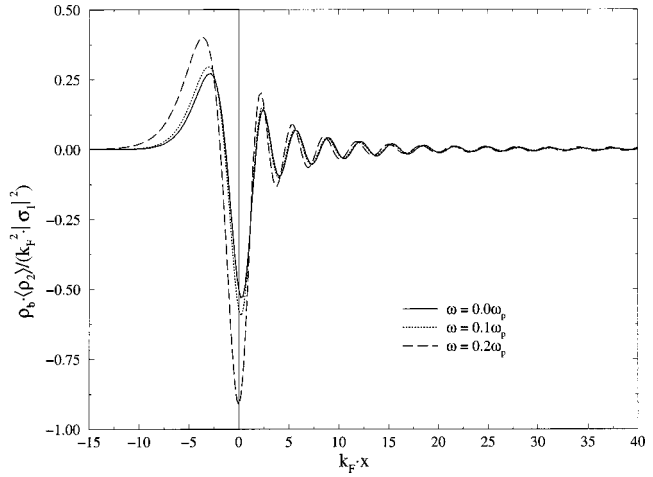

FIG. 2. Charge density from the nonretarded response calculation for $r_s=2$ at several frequencies of the applied field. The work function is about $0.23\omega_p$ for $r_s=2$.

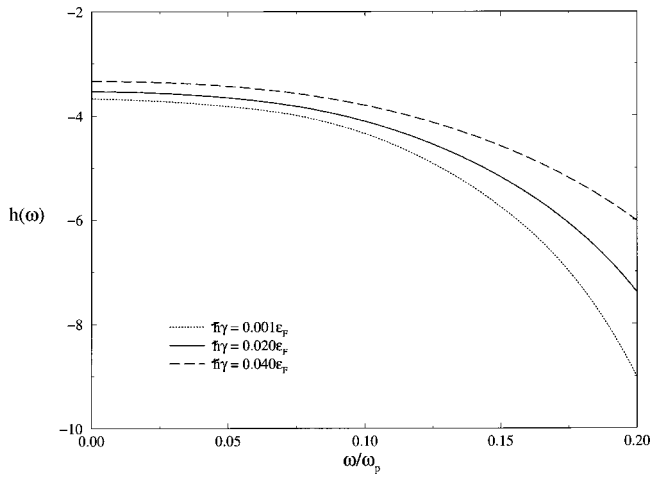

FIG. 3. Photon-drag h parameter versus frequency normalized to the bulk plasma frequency ω_p. Here $r_s=2$ and the global damping has the listed values. The use of Eq. (44) is especially important for the $\hbar\gamma=0.001\epsilon_F$ case.

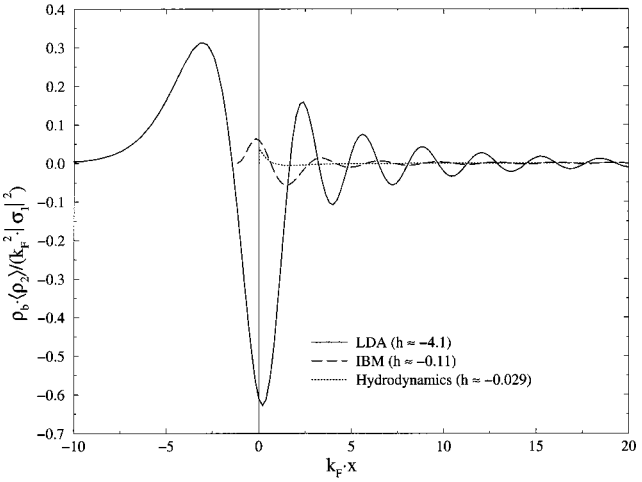

FIG. 4. Charge densities from nonretarded response calculations for $r_s=2$, $\hbar\gamma/\epsilon_F=0.02$, and $\omega/\omega_p=0.1$. The h parameter that results from each calculation is also given.

of the induced density $\rho_2(x,0)=\langle\rho_2\rangle$ that underlie the determination of h. The damping parameter is still 2% of the Fermi frequency and the induced charge disturbances are fairly well localized near the surface. The tail of Friedel oscillations is largely set by the static screening of $\rho_2(x,0)$ since it oscillates at $2k_F$. We have varied the bulk cutoff over the range $60<k_Fx_c<150$, and find little effect on the results. The numerical integral for $\sigma_2(0)=\int_{x_v}^{x_c}dx\rho_2(x,0)$ nearly vanishes. Specifically we find that $\sigma_2(0)/\int_{x_v}^{x_c}dx|\rho_2(x,0)|$ does not exceed a few percent for this case of bulk density and damping. The $\rho_2(x,0)$ do not dramatically change their shape as the driving frequency increases up to the photoemission threshold. There is also no qualitative difference between LDA and RPA results.[14]

At larger r_s or smaller damping our computer codes have difficulties, primarily due to the long range of Coulomb interactions and driving terms.[14] However, we have been able to reduce the anomalies by rescaling or shifting intermediate results in order to satisfy exact criteria. For instance, in linear response we find that our numerical σ_1 does not exactly satisfy Eq. (38), missing at worst by a few percent. Before calculating V_1 and V_2 and proceeding to the second-order calculation we rescale $\rho_1(x,\omega)$ so that its integral over x exactly matches Eq. (38). For the second-order response we similarly find that our computed ρ_2 does not satisfy Eq. (17). The resulting net charge on the surface can make the calculation of h or a unreliable. To remedy this error, we subtract from the computed ρ_2 a constant multiple of ρ_1 evaluated at $\tilde{\Omega}$:

$$\rho_2^{(\mathrm{impr})}(x,\tilde{\Omega})=\rho_2(x,\tilde{\Omega})-\lambda\rho_1(x,\tilde{\Omega}). \tag{44}$$

The parameter λ is chosen so the ''improved'' version of the second order density, $\rho_2^{(\mathrm{impr})}$, exactly satisfies Eq. (17). These modifications are of little consequence for larger values of the damping, say, $\gamma/\epsilon_F>0.02$ for $r_s=2$, but are crucial for allowing us to obtain a smooth and reasonable dependence of our results as $\gamma\to0$. The final results for h are roughly linear in γ, as illustrated in Fig. 3, which shows that there is more sensitivity to the choice of γ at larger frequencies. The general magnitude and frequency dependence of h do not, however, depend on the choice of γ.

IV. COMPARISONS

We finish by showing that different models of the electrons' behavior near the surface lead to quite different results. Figure 4 shows the photon-drag charge density determined in three separate ways for the same bulk density, damping, and applied frequency. The LDA curve is from Fig. 2 while the hydrodynamic result is produced from the theory of Ref. 3. We calculated the curve for the infinite barrier model (IBM) as a preliminary to setting up the LDA code.[14] For the IBM, the ground state potential energy V_0 is modeled by an infinite barrier located a distance $3\pi/8k_F$ beyond the edge of the jellium and its eigenstates are pure sine waves. This makes a RPA calculation of its response straightforward. The remarkable feature of Fig. 4 is how large the differences are between the predictions of the three

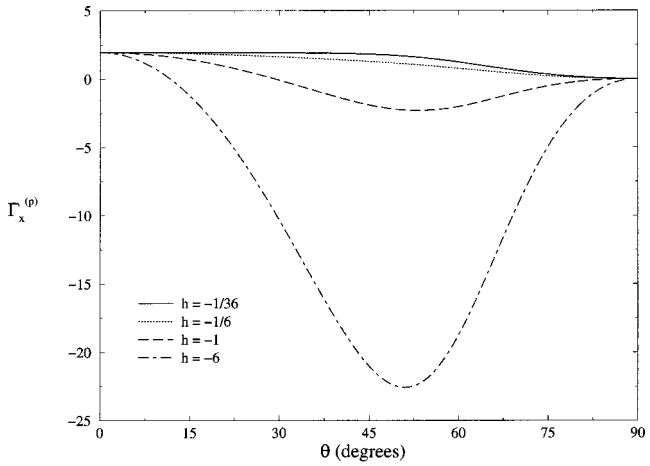

FIG. 5. Dimensionless voltage $\Gamma_x^{(p)}$ versus incident angle θ for p-polarized light. The light frequency is $\omega/\omega_p=0.1$ and the damping is $\gamma/\omega_p=0.015$. The different curves are calculated from Eq. (3) using the listed values of h.

models. The hydrodynamic ρ_2 has a discontinuity at the surface and of course lacks Friedel oscillations as one moves into the bulk. Its magnitude is also much smaller than either of the two quantum mechanical results. The two quantum results also differ considerably from each other. The LDA induced charge density is pulled much farther into vacuum and has stronger Friedel oscillations into the bulk. Clearly, ρ_2 is highly sensitive to the ground state density model, as expected.[2,15]

The associated values of h are also very different. For the LDA case, h is sufficiently negative to be able to change the sign of the induced voltage across the surface. This is illustrated in Fig. 5, which plots $\Gamma_x^{(p)}$ of Eq. (3) versus the angle of incidence for several possible values of h. For the typical size of h from hydrodynamic or IBM calculations, the voltage's sign never changes but the LDA results found here do lead to predicted sign changes. The experimental observation of such behavior would be an important confirmation of the contribution of h, which in turn should exhibit a strong dependence on surface conditions.

ACKNOWLEDGMENTS

Some of the calculations were done on the Cray Research Inc. T90 system at NPACI in San Diego, California. This work was also partially supported by the National Computational Science Alliance under Grant No. PHY 990009N and utilized the NCSA SGI/Cray Origin 2000.

[1] A. Liebsch and W. L. Schaich, Phys. Rev. B **40**, 5401 (1989).
[2] A. Liebsch, *Electronic Excitations of Metal Surfaces: Applications of Local Density Theory* (Plenum, New York, 1997).
[3] J. E. Goff and W. L. Schaich, Phys. Rev. B **56**, 15 421 (1997).
[4] V. L. Gurevich, R. Laiho, and A. V. Lashkul, Phys. Rev. Lett. **69**, 180 (1992).
[5] W. L. Schaich and A. Liebsch, Phys. Rev. B **37**, 6187 (1988).
[6] M. Zaluzny, Solid State Commun. **103**, 435 (1997).
[7] F. T. Vasko and O. Keller, Phys. Rev. B **58**, 15 666 (1998).
[8] S. V. Faleev and M. I. Stockman, Phys. Rev. B **59**, 7338 (1999).
[9] N. D. Lang, in *Solid State Physics*, edited by H. Ehrenreich, F. Seitz, and D. Turnbull (Academic, New York, 1973), Vol. 28, p. 225.
[10] A. L. Fetter and J. D. Walecka, *Quantum Theory of Many-Particle Systems* (McGraw Hill, Inc., New York, 1971).
[11] N. D. Lang and W. Kohn, Phys. Rev. B **7**, 3541 (1973).
[12] An analogous relation holds in first order: $\rho_1(x,-\omega) = \rho_1^*(x,\omega)$.
[13] G. Senatore and K. R. Subbaswamy, Phys. Rev. A **35**, 2440 (1987).
[14] For more details see J. E. Goff, Ph.D. thesis, Indiana University, 1999 (unpublished).
[15] P. J. Feibelman, Prog. Surf. Sci. **12**, 287 (1982).
[16] N. D. Mermin, Phys. Rev. B **1**, 2362 (1970).
[17] K. Kempa, A. Liebsch, and W. L. Schaich, Phys. Rev. B **38**, 12 645 (1988).
[18] The definitions of time Fourier amplitudes differ in Refs. 1 and 2 from those used here.
[19] N. W. Ashcroft and N. D. Mermin, *Solid State Physics* (Saunders, New York, 1976).